Structural and spectroscopic in vivo imaging of the human retina with scanning light ophthalmoscopy

Damodaran, M.

2020

document version
Publisher's PDF, also known as Version of record

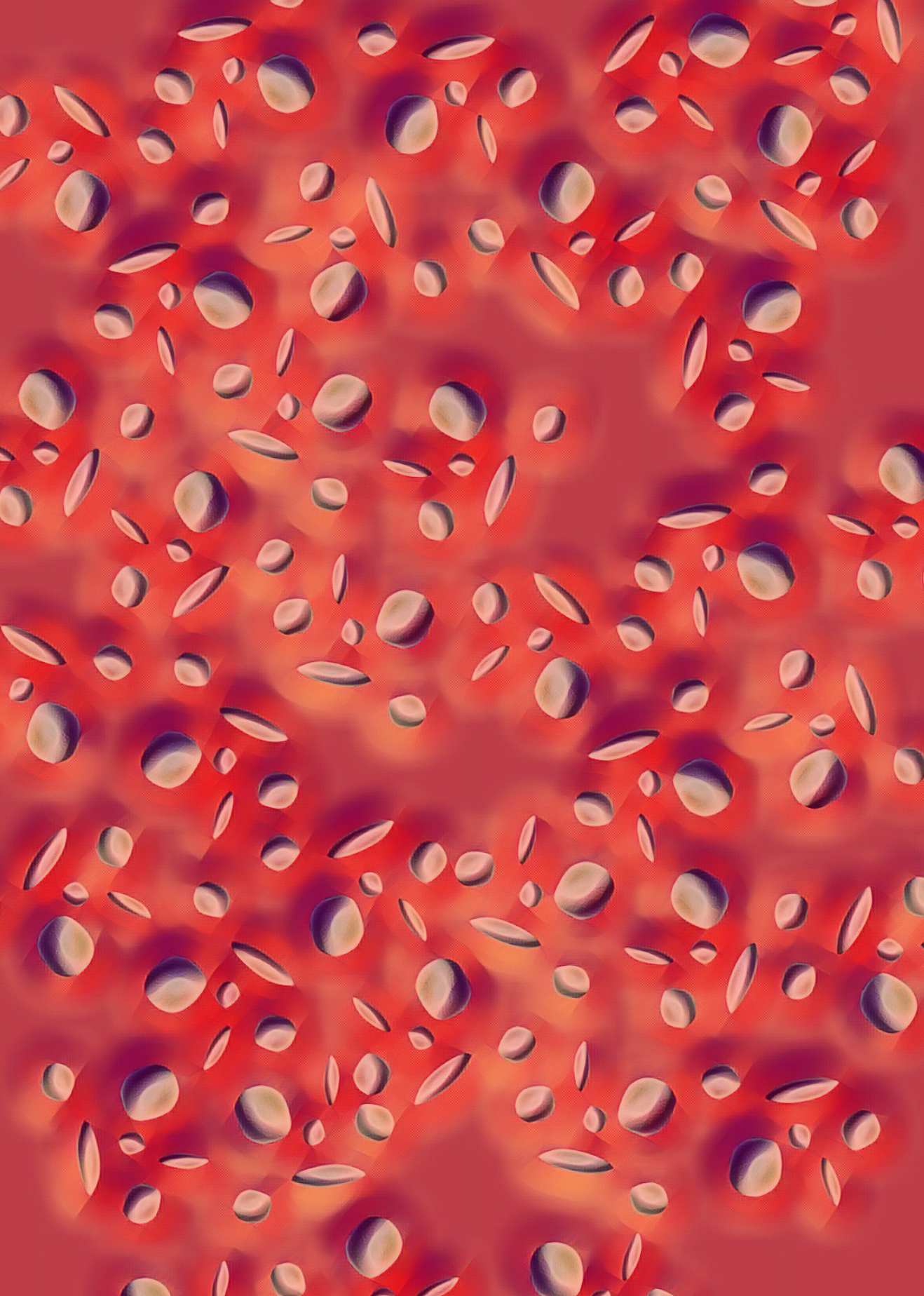

6

Non-invasive optical measurement of haemoglobin concentration in the posterior eye of adult humans

based on:

M. Damodaran, A. Amelink, and J. F. de Boer, "Non-invasive optical measure-ment of haemoglobin concentration in the posterior eye of adult humans" (manuscript in preparation).

Abstract

Haemoglobin concentration in blood is an important biomarker. Current methods to measure blood haemoglobin concentration involves the invasive procedure of drawing blood from a vein or through a finger prick. In this letter, a non-invasive spectrophotometric method to image the retina simultaneously at two isosbestic wavelengths and to extract the haemoglobin concentration values from the two images is presented. We have measured the haemoglobin concentration in human retinas using a dual-wavelength scanning laser ophthalmoscope that uses a supercontinuum light source, and a balanced detection scheme. The optimum wavelength combination (522 nm and 548 nm) for the measurement was chosen based on an error propagation analysis.

6.1 Introduction

Haemoglobin (Hb) concentration in blood is used for many applications in the medical field, e.g. for anaemia diagnosis [1], to screen blood donors, and in transfusion guidance. The need to draw blood for Hb concentration for analysis is undesirable for several reasons, including discomfort to the patient, the time required of medical personnel to draw and handle the samples, and the potential risk of spreading blood-borne diseases through punctures of the skin. Repeated drawing of blood samples and *in vitro* analysis is especially undesirable in infants, in situations with blood loss, and low resource settings in developing countries. Several methods attempting non-invasive Hb concentration quantification have been investigated previously [2]. These methods are mostly based on measurements in skin extremities such as the fingertip or earlobe [3, 4] and require extensive calibration due to the lack of direct visual access to blood vessels. Further, studies assessing the accuracy of point-of-care tests [5] have found high variability in Hb concentration obtained from successive drops of fingerpick blood. Both Hb concentration and haematocrit are used for the diagnosis of anaemia. They are related through the mean corpuscular haemoglobin concentration, which is assumed to be 32 to 36 [g/dL] for human blood [6]. Thus, Hb concentration in g/dL can be approximately converted to haematocrit in % by multiplying Hb concentration by 3. However, the Hb concentration is more stable to plasma volume changes such as dehydration, which makes it more reliable for the assessment of anaemia [7]. The eye provides a unique location in the human body with visual access to blood vessels. The blood vessels in the retina are located very superficially, are optically well accessible, and thus provide a unique access point for Hb concentration estimation

due to the lack of thick overlying tissues present elsewhere in the body [8]. The ophthalmic artery, which supplies blood to the eye, is the first branch of the internal carotid artery and any global variation in Hb concentration in the body is expected to be measurable in the retinal vessels close to the optic nerve head (ONH). In the retina, haematocrit quantification by performing in vivo imaging was previously explored using optical coherence interferometry (OCT) methods either by fitting the attenuation slope of the OCT signal [9] centred at 830 nm or by fitting Visible OCT angiogram signals [10]. A direct spectrophotometric method to measure haematocrit has been conceptualised [11] but has not yet been demonstrated. In this letter, we demonstrate Hb concentration estimation using a novel scanning laser ophthalmoscope (SLO) design which uses a supercontinuum light source for imaging the retina simultaneously at two wavelength bands.

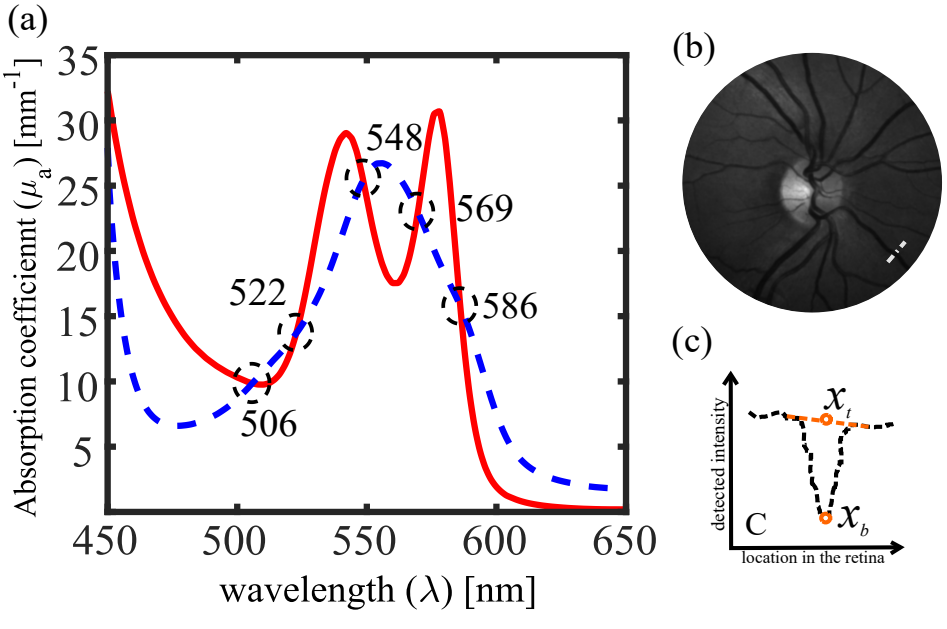

Figure 6.1: (a): Absorption spectrum of oxy- and deoxy- Hb in the [450 650] nm range showing the various isosbestic points where the absorption is independent of the oxygenation of the Hb molecule. (b): in vivo retinal image at (λ = 570 $\pm$ 30 nm) obtained using a fundus camera. (c): A line profile along a blood vessel to extract the reflectance value at tissue and blood vessel locations.

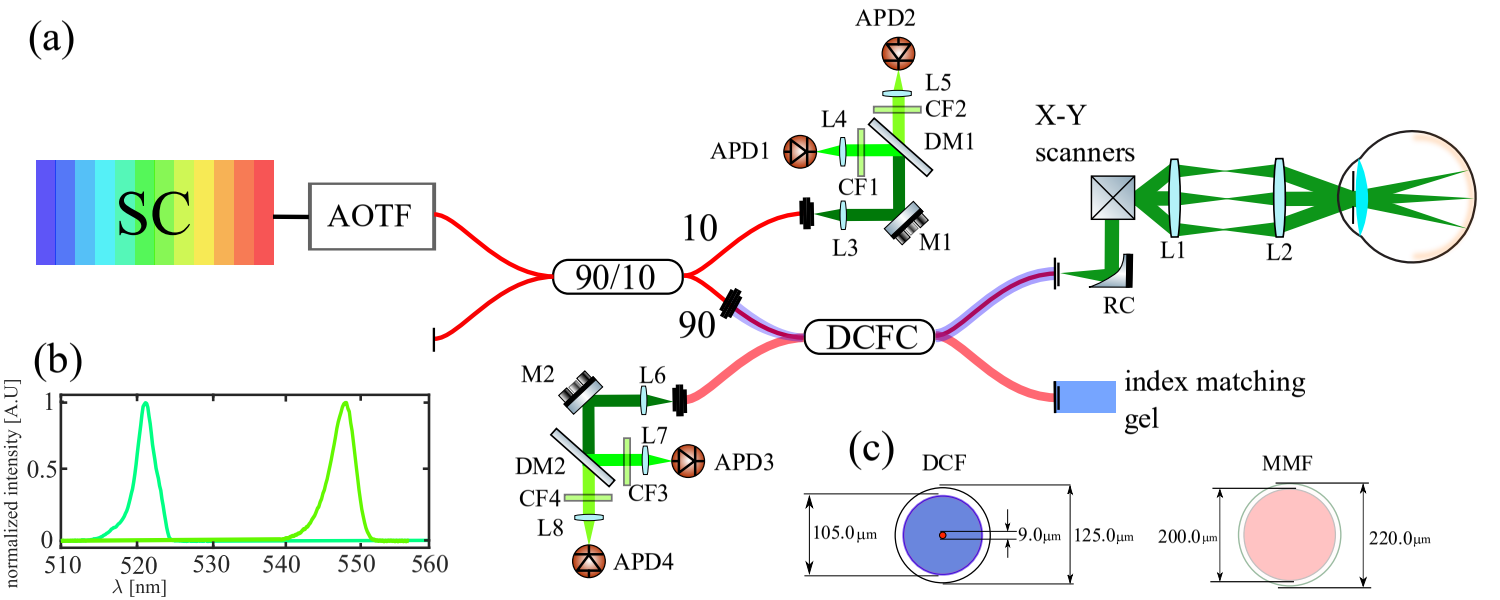

Figure 6.2: (a): Schematic of the setup: Light from a supercontinuum source (SC) (EXU-6, NKT Photonics A/S, Birkerød, Denmark) was filtered using an acousto optic tunable filter (AOTF) (Select, NKT Photonics A/S, Birkerød, Denmark). A 90:10 coupler (TW560R2A2, Thorlabs GmbH, Germany) was used to split off 10 % of the light for balanced detection. The 90 % port of the splitter was coupled to the core of a double-clad fibre (DCF) in the DCF coupler (DCFC). About 94 % (transmission measured at 550 nm) of this light reached the pupil plane. L1-L8: Lenses, M1-M2: Mirrors, CF1, CF3: bandpass clean-up filters, CF2, CF4: 532 nm long pass clean-up filters, APD1-APD4: Avalanche photodiodes (APD410A2, Thorlabs GmbH, Germany). D1, D2: Dichroic beam splitters (long pass 532 nm), RC: Reflective collimator (RC02APC-P01, Thorlabs GmbH, Germany). (b): Illumination spectrum of the wavelengths 522nm (FWHM: 2.2 nm) and 548 nm (FWHM: 3.7 nm) used for imaging. (c): Configuration of the DCF and multimode fibre (MMF) used in the setup. The DCF had a core numerical aperture (NA) of 0.11. The NA of the inner cladding was 0.22, and the inner cladding of the DCF was coupled to an MMF with NA of 0.22.

6.2 Methods

Figure 6.1a shows the Hb absorption spectrum, which varies for most wavelengths based on the oxygenation of Hb except for isosbestic wavelengths [12]. The effect of optical absorption of Hb on image formation is visible in Fig. 6.1b where the blood vessels look significantly darker compared to the surrounding tissue. The attenuation of light due to the presence of Hb can be used to determine the concentration of Hb within the vessel using a non-invasive reflectance measurement at two isosbestic wavelengths. A typical method for measuring the absorbance of blood at a particular blood vessel in the retina is shown in the inset of Fig. 6.1c where the intensity profile of the blood vessel (dotted line) is plotted as a function of the location on the retina. If $I(\overline{x}_b, \lambda)$ and $I(\overline{x}_t, \lambda)$ are the recorded intensities in the retinal image at the centre of the blood vessel and adjacent tissue location respectively at a wavelength λ, and the incident light intensity was the same at both locations, the relative optical density OD_λ of blood vessel location compared to the surrounding tissue at a particular wavelength can be written as [13],

$$OD_\lambda = \ln\Big(\frac{I(x_t,\lambda)}{I(x_b,\lambda)}\Big) = \langle L_{eff}(\lambda)\rangle \cdot \big(S \cdot \mu_a^{HbO_2}(\lambda) + (1-S)\cdot \mu_a^{Hb}(\lambda)\big) + G(\lambda) \quad (6.1)$$

where the attenuation of the reflected light due to the blood within $\overline{x}_b$ is governed by *modified Beer-Lamberts law* [14] with $\langle L_{eff}(\lambda)\rangle$, the effective path length of photons travelling through the probed volume before reaching the detector. S is the oxygen saturation of blood defined as the ratio of amount of oxy-haemoglobin to the total haemoglobin. The absorption coefficients of oxy- and deoxy-Hb are given by $\mu_a^{HbO_2}(\lambda)$ and $\mu_a^{Hb}(\lambda)$, respectively, and the oxy and deoxy absorption coefficients are the product of the respective molar extinction coefficients, ($\epsilon_{HbO_2}(\lambda)$, $\epsilon_{Hb}(\lambda)$) and the concentration of Hb (c_{Hb}). $G(\lambda)$ is a factor which accounts for any apparent increase or decrease in the ODs purely due to scattering differences within the volumes $\overline{x}_b$ and $\overline{x}_t$. If λ_1 and λ_2 are isosbestic wavelengths (see Fig.6.1a) i.e., $\mu_a^{HbO_2}(\lambda) = \mu_a^{Hb}(\lambda) = \mu_a^i(\lambda)$, Eq. 6.1 can be written as,

$$OD_{\lambda_i} = \langle L_{eff}(\lambda_i)\rangle \cdot \mu_a(\lambda_i) + G(\lambda_i) \quad (6.2)$$

We have previously described a novel multi-color scanning laser ophthalmoscope (mcSLO) that uses a supercontinuum source and variable line pass filter to perform retinal oximetry [15]. We here use the same system to perform the first proof of principle measurements of haemoglobin concentration in human retinas. In this double clad fiber (DCF) coupler based SLO shown in Fig. 6.2, only

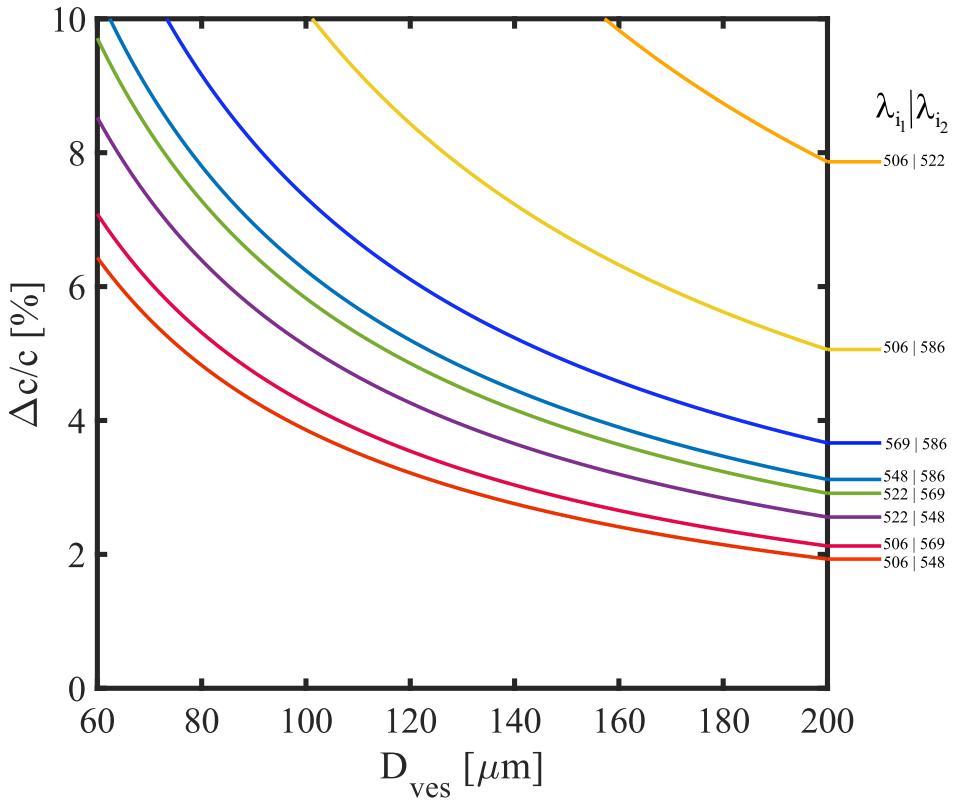

Figure 6.3: The percentage error (0 to 10%) in Hb concentration estimation for different wavelength combinations of isosbestic points assuming an SNR of 20 dB in the retinal images and a standard error in estimating the blood vessel diameter to be 10 µm. The most optimum wavelength combination is 506, 548 nm where the difference in absorption of Hb among these wavelengths is the highest (see Fig. 6.1a).

the light from the cladding is coupled to the multimode fiber, and the direct back scattered light from the retina, which travels through the core, does not reach the detector [16]. We demonstrated that the effective path length $\langle L_{eff} \rangle$ of the detected photons have the following linear relationship with the blood vessel diameter for 70 µm $\leq D_{ves} \leq$ 150 µm : $\langle L_{eff} \rangle$[mm] = (0.46·D_{ves}+0.0052)[mm] [15]. Since $\mu_a = \ln 10 \cdot \epsilon(\lambda) \cdot c_{Hb}$, and the molecular weight of Hb is 64500 g/mol we can write the Hb concentration (c_{Hb}) as,

$$c_{Hb}\,[\mathrm{g/L}] = \frac{(OD_{\lambda_{i1}} - OD_{\lambda_{i2}})[-] \times 64500[\mathrm{g/mol}]}{\ln(10) \cdot (0.46 \cdot D_{ves} + 0.0052)[\mathrm{mm}] \cdot \left(\epsilon_a^i(\lambda_{i1}) - \epsilon_a^i(\lambda_{i2})\right)[\mathrm{L/mol/mm}]} \tag{6.3}$$

We can further determine optimum 'isosbestic' wavelength combination for es-

timating c_{Hb} from the ten combinations possible in [500 600] nm range by performing an error propagation analysis on Eq. 6.3. Figure 6.3 shows the results of this error analysis assuming an SNR of 20 dB in the intensities of the images (corresponding to 1% measurement noise) and uncertainty in vessel diameter estimation of 10 µm. Based on the analysis, 506 nm and 548 nm (largest absorption contrast) are the best wavelength combination for accurate c_{Hb} estimation. Nevertheless, we prefer the 522 and 548 nm combination since the wavelengths are closer (26 nm vs 42 nm separation). Therefore, the difference in wavelength-dependent scattering properties will be smaller, i.e., the difference in the factor $G(\lambda)$ will be smaller, and as a consequence, the wavelength dependence is expected to cancel out better when taking a difference of ODs in Eq. 6.1. The error analysis demonstrates that for the 522 and 548 nm combination the error in C_{Hb} measured in large blood vessels is only slightly higher than for the 506-548 pair and still within 5% for D_{ves} ≥100 µm. For 522-548 nm combination, The c_{Hb} concentration (from Eq. 6.3) becomes

$$c_{Hb}\,[\mathrm{g/dL}] = \frac{1.3[] \times (OD_{\lambda_{i1}} - OD_{\lambda_{i2}})}{(0.46 \cdot D_{ves} + 0.0052)[\mathrm{mm}]} \tag{6.4}$$

The mcSLO (Fig. 6.2) is capable of simultaneous imaging at two different wavelengths. A combination of a 2.56 kHz resonant scanner (5.12 kHz line rate by utilising both directions of scanner sweep) (EPOC., Glendale, New York, USA), and a 10 Hz galvanometer mirror (Cambridge tech., Bredford, USA) placed close to each other were used to achieve an imaging throughput of 10 frames/second. The field of view (FOV) of the images was controlled by the voltage (amplitude) supplied to the scanning mirrors. The reflected and scattered light from the retina was then collected using the inner cladding of the double-clad fibre in port A. About 63 % (transmission measured at 550 nm) of the collected light is then coupled on to the multimode fibre (MMF) which is detected using two APDs and suitable filters to separate the 522 nm and 548 nm channels. The SC source results in noise in the images dominated by relative intensity noise (RIN). To reduce the RIN noise, balanced detection was implemented by simultaneously detecting the illumination signal, as shown in Fig. 6.2. As shown in 6.4, balanced detection resulted in a 6 dB and 7 dB signal to noise ratio improvement for 522 nm and 548 nm images, respectively [15].

The *in vivo* study obeyed the principles of the Declaration of Helsinki and was approved by the Institutional review board at the VU Medical Centre, Amsterdam. Tropicamide 0.5 % w/v. eye drops were administered before imaging the volunteers to obtain better collection efficiency through the pupil of the eye. This was essential because of the involuntary response of the pupil that constricts due to a bright light reflex. Dual-wavelength images were acquired from healthy vol-

unteers. The optical power used for measuring human subjects was 150 µW per wavelength, and this was in agreement with the maximum permissible power prescribed by the IEC standard 60825-1 [17] for 8 hours of continuous exposure. Before recording the images, a reference measurement of the internal system reflections and background was recorded. Each background-subtracted frame containing both the forward and backward direction of the sweep of the resonant scanner was de-interleaved and dewarped. The images showed negligible corneal reflections and were artefact-free except for a strong lens reflection (L2 in Fig. 6.2), which saturated the detector. Consecutive frames were registered and averaged to improve the SNR and image contrast further. Given the improvement in SNR of the images with balanced detection, averaging 10 frames was sufficient to achieve an SNR 20 dB in the blood vessel and tissue locations. The vessel segmentation was done using retinal segmentation package (ARIA) based on wavelets and edge location refinement [18].

The Hb concentration was analysed in blood vessels with diameters $\geq$ 70 µm. The I($\overline{x}_b$,λ) and I($\overline{x}_t$,λ) were acquired for each location in the centre of the blood vessel and surrounding tissue as described previously [13]. The corresponding ODs were estimated, and the Hb concentration was calculated from Eq. 6.4. The *in vivo* imaging results from the right eyes of three healthy human volunteers is shown in Fig. 6.6. The left panel of Fig 6.6 shows the 522 nm image, and the middle panel shows the 548 nm image overlaid with blood vessel segmentation and the Hb estimation. The right panel of Fig. 6.6 shows the Hb concentration (mean value with error bar) estimated for each labelled blood vessel in the middle panel. The Hb concentration was shown only for parts of some vessels for the following reasons: (i) The automated vessel segmentation package (ARIA) [18] was found to be unreliable for vessel crossings, as well as in the edges of the image. (ii) For vessels, which are close to each other, there is not enough 'vessel-free tissue' to average the tissue intensity $I(x_t, \lambda)$ values in Eq. 6.1 to obtain proper estimates of the ODs of the tissue locations adjacent to the vessels.

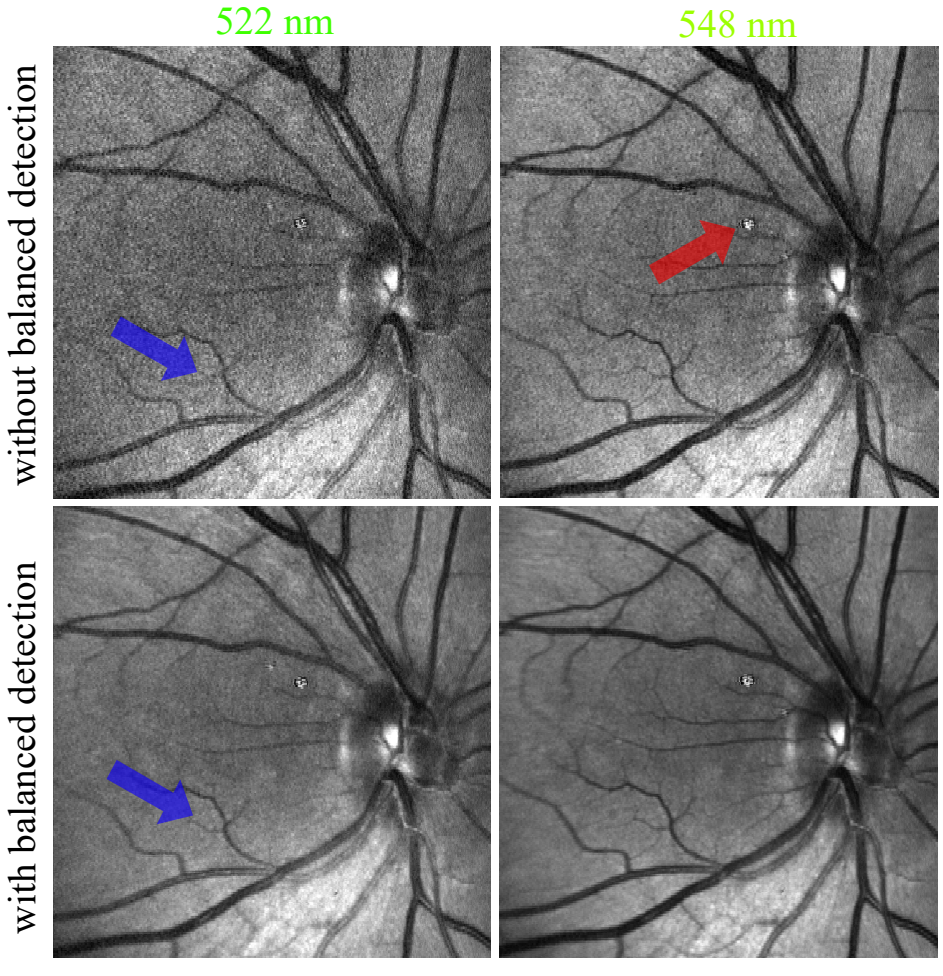

Figure 6.4: Single-frame balanced and unbalanced images from the 522 nm and 548 nm channels clearly show the improvement in image quality achieved by implementing balanced detection. Specific example is the small blood vessel (blue arrow) in the 522 nm channel visible only with balanced detection. The bright central reflection (red arrow) from the lens L1 (see Fig. 2a) was let to saturate the detector so as not to compromise the dynamic range of the image.

6.3 Results and discussion

The estimated mean Hb concentration in the right eye of a healthy volunteer (male, 45 years) was 15.5 ± 0.7 [g/dL].

These extracted values of Hb concentration agree with the physiologically expected values as reported in the literature. These values were derived using an effective path length $\langle L_{eff} \rangle$ that was extracted from a hyperspectral measurement

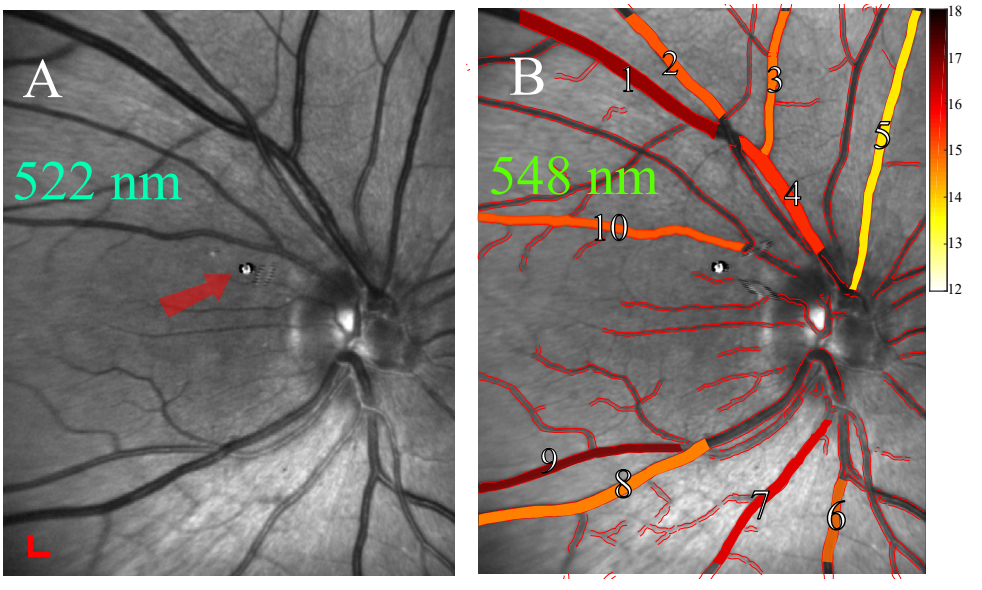

Figure 6.5: Hb concentration estimation in adult human volunteer — The 522 nm (A) and 548 nm (B) retinal image is shown for each volunteer. The vessels with diameters $\geq$ 65 µm near the ONH was analysed, and an image overlay showing the Hb concentration estimates as a colormap on the *in vivo* image is shown (B). The value for each individual vessel is also plotted, with the overall mean and standard deviation shown in red. Scale bar represents 300 µm in each direction.

over 484 to 608 nm in a single volunteer where a haemoglobin concentration of c = 15 g/dL was assumed, and $\langle L_{eff} \rangle$ and oxygen saturation S were fitted to the hyperspectral data [15]. However, the exact relation between $\langle L_{eff} \rangle$ and blood vessel diameter and its wavelength dependence deserves further investigation.

We observe intra-retinal variations in Hb concentration within the retina of the volunteer. Although it is hard to find literature that suggests how Hb concentration varies with vessel diameter, we had expected to find a relatively homogeneous distribution of Hb concentration throughout all the (large) vessels in the retina. The observed variations in Hb concentration estimation between different vessels and vessel segments may be caused, e.g. by variations in the depths and angles of the vessels with respect to the tissue surface, or by the presence of a central light reflex, which makes it difficult to estimate the OD in the centre of the vessel. These issues deserve further investigation. Despite the observed variations within each image, averaging the results of all the vessels gives a reasonable estimate of the systemic Hb concentration, which is the parameter of interest.

The error in the overall Hb concentration was around 0.7 [g/dL] when averaged over 10 blood vessels. This is better than the error on previously reported

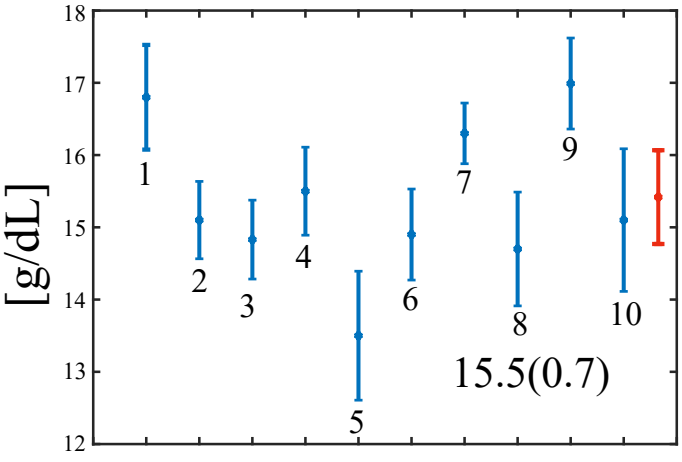

Figure 6.6: Hb concentration estimation in adult human volunteer — The 522 nm (A) and 548 nm (B) retinal image is shown for each volunteer. The vessels with diameters $\geq$ 65 µm near the ONH was analysed, and an image overlay showing the Hb concentration estimates as a colormap on the *in vivo* image is shown (B). The value for each individual vessel is also plotted, with the overall mean and standard deviation shown in red. Scale bar represents 300 µm in each direction.

values [9, 10] on Hb concentration in the retina. Since the Hb concentration estimation was performed in large, superficial blood vessels in the retina, the pigment packaging effect [19, 20] is not expected to play a significant role in the effective blood vessel absorption. Although the method of haemoglobin concentration estimation from retinal images has been demonstrated with a complex, expensive mcSLO setup, the method could be translated into an application setting using a simpler and compact prototype. For example, a fundus camera employing low-cost hardware [21] and LEDs or filters with transmission windows corresponding to the optimum wavelengths could be implemented. This would not only bring a cost and device simplicity advantage but also remove the complex dependence of $\langle L_{eff} \rangle$ on blood vessel diameter and wavelength as found for our sub-diffuse SLO imaging scheme. Instead, for a fundus camera the relation $\langle L_{eff} \rangle = D_{ves}$ [22] holds, which could simplify the analysis of haemoglobin concentration compared to the SLO implementation.

6.4 Conclusion

In summary, the first results are shown from an experimental SLO system that uses an SC light source to produce multiple high contrast reflectance images of the retina

simultaneously at two wavelengths at a speed of 10 fps. The SLO based on an SC source is very promising for spectral visualisation of the posterior part of the eye at high acquisition speeds with good resolution and contrast. Though the SC source has RIN noise, the acquired quasi-confocal images show superior contrast and quality thanks to the balanced detection scheme, which significantly reduced the RIN noise and improved the SNR. Since the SC source can be used to output any wavelength(s) of choice between 450 nm and 2400 nm, it offers numerous possibilities for obtaining spectral signatures of the retina including retinal oximetry, autofluorescence imaging and RPE melanin absorption characterisation. This might be very helpful for the detection of new pathological structural and functional changes in the retina. Although the demonstration of the method has been done with the sophisticated setup in Fig. 2, the method can be translated to clinics, and for field applications using a simpler and compact prototype. For example, a fundus camera employing low-cost hardware [21], and filters with transmission windows corresponding to the optimum wavelengths could be implemented for clinical applications. Fundus cameras also satisfy the requirement of the photon path lengths being approximately equal to the diameter of the blood vessels [22].

References

[1] R. D. Tyler and R. L. Cowell, "Classification and Diagnosis of Anaemia," Comp. Haematol. Int. 6, 116 (1996).

[2] J. W. Mcmurdy, G. D. Jay, S. Suner, and G. Crawford, "Noninvasive Optical, Electrical, and Acoustic Methods of Total Hemoglobin Determination," Clin. Chem. 54, 264272 (2008).

[3] S. Kim and J. Kim, "Noninvasive total hemoglobin measurement," J. Biomed. Opt. 7, 4550 (2002).

[4] A. Sakudo, Y. Hakariya, H. Kuratsune, and K. Ikuta, "Non-invasive prediction of hematocrit levels by portable visible and near-infrared spectrophotometer," Clin. Chim. Acta 408, 123127 (2009).

[5] M. M. Bond and R. R. Richards-Kortum, "Drop-to-drop variation in the cellular components of fingerprick blood: Implications for point-of-care diagnostic development," Am. J. Clin. Pathol. 144, 885894 (2015).

[6] RBC indices: MedlinePlus Medical Encyclopedia, (2019).

[7] L. Quintó, J. J. Aponte, C. Menéndez, J. Sacarlal, P. Aide, M. Espasa, I. Mandomando, C. Guinovart, E. Macete, R. Hirt, H. Urassa, M. M. Navia, R. Thompson, and P. L. Alonso, "Relationship between haemoglobin and haematocrit in the definition of anaemia," Trop. Med. Int. Heal. 11, 12951302 (2006).

[8] J. Mcmurdy, G. Jay, S. Suner, and G. Crawford, "Photonics-based In Vivo total hemoglobin monitoring and clinical relevance," J. Biophotonics 287, 277287 (2009).

[9] N. V. Iftimia, D. X. Hammer, C. E. Bigelow, D. I. Rosen, T. Ustun, A. A. Ferrante, D. Vu, and R. D. Ferguson, "Toward noninvasive measurement of blood hematocrit using spectral domain low coherence interferometry and retinal tracking," Opt. Express 14, 3377 (2006).

[10] S. P. Chong, M. Bernucci, H. Radhakrishnan, and V. J. Srinivasan, "Structural and functional human retinal imaging with a fiber-based visible light OCT ophthalmoscope," Biomed. Opt. Express 8, 323 (2017).

[11] M. J. Rice, R. H. Sweat, W. T. William, and W. Routt, "Non-invasive measurement of blood component using retinal imaging," United States Pat. US6305804B1 (2001).

[12] N. Bosschaart, G. J. Edelman, M. C. G. Aalders, T. G. van Leeuwen, and D. J. Faber, "A literature review and novel theoretical approach on the optical properties of whole blood," Lasers Med. Sci. 29, 453479 (2014).

[13] M. Damodaran, A. Amelink, and J. F. de Boer, "Optimal wavelengths for subdiffuse scanning laser oximetry of the human retina," J. Biomed. Opt. 23, 1 (2018).

[14] A. Sassaroli and S. Fantini, "Comment on the modified Beer-Lambert law for scattering media," Phys. Med. Biol. 49, (2004).

[15] M. Damodaran, A. Amelink, F. Feroldi, B. Lochocki, V. Davidoiu, and J. F. de Boer, "In vivo subdiffuse scanning laser oximetry of the human retina," J. Biomed. Opt. 24, 1 (2019).

[16] E. De Montigny, W.-J. Madore, O. Ouellette, G. Bernard, M. Leduc, M. Strupler, C. Boudoux, and N. Godbout, "Double-clad fiber coupler for partially coherent detection," Opt. Express 23, 90409051

(2015).

[17] International Electrotechnical Commission, "International Electrotechnical Commission, Safety of Laser Products Part 1: Equipment Classification and Requirements, (Geneva, Switzerland), IEC-60825-1 (2014)," 122 (2014).

[18] P. Bankhead, C. N. Scholfield, J. G. McGeown, and T. M. Curtis, "Fast retinal vessel detection and measurement using wavelets and edge location refinement," PLoS One 7, 112 (2012).

[19] N. Rajaram, A. Gopal, X. Zhang, and J. W. Tunnell, "Experimental validation of the effects of microvasculature pigment packaging on in vivo diffuse reflectance spectroscopy," Lasers Surg. Med. 42, 680688 (2010).

[20] J. C. Finlay and T. H. Foster, "Effect of pigment packaging on diffuse reflectance spectroscopy ofsamples containing red blood cells," Opt. Lett. 29, 965967 (2004).

[21] M. Damodaran, K. V. Vienola, B. Braaf, K. A. Vermeer, and J. F. de Boer, "Digital micromirror device based ophthalmoscope with concentric circle scanning," Biomed. Opt. Express 8, (2017).

[22] P. I. Rodmell, J. A. Crowe, A. Gorman, A. R. Harvey, G. Muyo, D. J. Mordant, A. I. McNaught, and S. P. Morgan, "Light path-length distributions within the retina," J. Biomed. Opt. 19, 036008 (2014).